Journal of Power Sources 660 (2025) 238548

Contents lists available at ScienceDirect

Journal of Power Sources

journal homepage: www.elsevier.com/locate/jpowsour

Development and characterization of laboratory-scale sodium-ion battery full cell containing low fluorinated electrolyte

Muhammad Nouman Aslam [a], Yiyue Lu [a], Shuting Zhang [b,c], Mariana Gaško [b,c], Maider Zarrabeitia [b,c], Lukas Fridolin Pfeiffer [d], Timo Werner [d], Peter Axmann [d], Christian Leibing [a], Andrea Balducci [a,*]

[a] Institute of Technical and Environmental Chemistry, Friedrich Schiller University Jena and Center for Energy and Environmental Chemistry (CEEC) Jena, Philosophenweg 7a, 07743, Jena, Germany
[b] Helmholtz Institute Ulm (HIU), Helmholtzstrasse 11, 89081, Ulm, Germany
[c] Karlsruhe Institute of Technology (KIT), 76021, Karlsruhe, Germany
[d] ZSW Center for Solar Energy and Hydrogen Research Baden-Württemberg, Lise-Meitner-Strasse 24, 89081, Ulm, Germany

HIGHLIGHTS

- The combined use of NaFSI and NaDFOB allows the design of advanced electrolytes.
- NIB full cells containing this low-fluorine electrolyte display high performance.
- The combined use of NaFSI and NaDFOB allows the formation of effective interphases.

ARTICLE INFO

Keywords:
Sodium-ion battery
Low-fluorinated electrolyte
Sodium bis(fluorosulfonyl)imide
Sodium difluoro(oxalato)borate

ABSTRACT

Sodium-ion batteries (NIBs) are increasingly recognized as a viable and complementary technology to the Li-ion batteries (LIBs), with progress towards commercialization. However, the performance, stability and safety of these devices need to be further improved. State-of-the-art electrolytes, containing high fluorine content such as sodium hexafluorophosphate ($NaPF_6$), guarantee satisfactory performance with improved SEI stability, but they pose serious environmental and safety concerns. Therefore, the development of less-fluorinated electrolytes that offer safe, sustainable, and promising performance is immensely important. This study investigates a sustainable, low-fluorinated electrolyte, comprising sodium bis(fluorosulfonyl)imide (NaFSI) and sodium difluoro(oxalato) borate (NaDFOB) in propylene carbonate (PC) solvent, for NIBs. The findings underscore that the use of this electrolyte in a laboratory-scale NIB full cell containing hard carbon (HC) and P2-$Na_{2/3}Al_{1/9}Fe_{1/9}Mn_{2/3}Ni_{1/9}O_2$ (P2-AFMNO) cathode, allows the realization of devices which display high performance and stability, i.e., achieving 80 % capacity retention within a wider voltage range of 1.5–4.3 V vs Na^+/Na, after 200 cycles. An X-ray photoelectron spectroscopy (XPS) analysis revealed the formation of inorganic-rich, robust and stable interfaces on both electrodes, contributing to enhanced stability and lifetime of the NIB demonstrator.

1. Introduction

NIB technology has become one of the most matured contenders in the pursuit of "beyond LIB" technologies, approaching the stage of commercialization [1–3]. Over the past decade, the growing societal demand for sustainable battery solutions has led scientists to investigate alternatives to LIBs [1,4]. Throughout this exploration, the advantages of sodium resources such as their abundance, homogenous distribution, lower cost of precursor materials (Na_2CO_3), and higher safety, have also attracted industrial interest, positioning NIBs as a viable and complementary technology to LIBs [2,3,5–7]. Moreover, it also highlights the feasibility of technology transfer using the existing LIBs infrastructure to enable large scale NIBs production. Although continuous efforts are being made to boost the energy density of NIBs to complement LIBs for

This article is part of a special issue entitled: In memory of Professor Bruno Scrosati published in Journal of Power Sources.

* Corresponding author.
E-mail address: andrea.balducci@uni-jena.de (A. Balducci).

https://doi.org/10.1016/j.jpowsour.2025.238548
Received 25 June 2025; Received in revised form 11 September 2025; Accepted 29 September 2025
Available online 4 October 2025

electric mobility, today's NIBs already offer practical stationary storage solutions in applications where weight or volume constraints are less stringent [3,8–10].

State-of-the-art NIBs in a typical configuration use a carbonaceous material anode typically hard carbon (HC), with an insertion type cathode material depending on the area of application. For high power (W/kg) devices, Prussian blue/white analogues and sodium polyanions compounds are the leading candidates providing longer lifetimes, in contrast to sodium layered oxides, which ensure relatively higher energy density (Wh/kg) with good cycle life [11–21]. The state-of-the-art NIBs use analogous advanced LIBs electrolyte, having dissolved $NaPF_6$ conducting salt in carbonate-based solvents such as propylene carbonate (PC) and ethylene carbonate (EC) [22–29]. Although significant progress has been witnessed in the past recent years regarding the development of high capacity and high voltage materials for NIBs, the stability of NIBs operating at high voltage (>4 V vs Na^+/Na) still poses a major bottleneck [30]. Furthermore, the presence of $NaPF_6$, although it guarantees the formation of an effective SEI, limits the safety of these devices. As a matter of fact, $NaPF_6$ produces highly toxic and corrosive HF (produced by the highly reactive PF_5 with any trace amounts of moisture). Additionally, the emission of toxic fluoride gases, i.e., HF or POF_3, during battery fires can aggravate the safety risks, especially in confined areas of electric vehicles [31–33]. Considering the potential hazards posed by high fluorine content salt electrolytes such as $NaPF_6$ and given the environmental persistence of C-F bonds in sodium bis (trifluoromethyl sulfonyl) imide (NaTFSI) for extended periods [34], the necessity of low fluorinated novel electrolytes which support the safe and sustainable future of NIBs becomes clear. In this context, it has been shown that the combined use of NaFSI and borate-based NaDFOB is a promising approach to meet these requirements. NaFSI exhibits good solubility and thermal stability in carbonate-based solvents but has a limited ability to prevent the corrosion/dissolution of Al current collector at high voltages [35,36]. In contrast, NaDFOB forms an effective SEI passivation film and prevents Al dissolution but shows lower solubility in carbonate solvents [37–39]. Recently, a study was conducted by Xia's group focusing on the dual-salts combination where they reported interesting results when combining 0.8 M NaFSI +0.2 M NaDFOB in EC: PC (1:1, v/v) with phosphate-based $Na_3V_2(PO_4)_3$ cathode [40]. In a recent work, our group extensively discussed how the combination of these salts helped suppress the Al current collector dissolution, and its use allows high and stable performance for high voltage layered oxide cathode (P2-$Na_{2/3}Al_{1/9}Fe_{1/9}Mn_{2/3}Ni_{1/9}O_2$) [41].

Herein, we investigate the use of the electrolyte 0.5 M NaFSI + 0.5 M NaDFOB in PC, which in our previous study has been identified as the most promising mixture [41], in NIBs. Initially, the performance and compatibility of HC in this electrolyte was investigated. Afterwards, a lab scale NIB full cell was assembled utilizing HC in combination with P2-$Na_{2/3}Al_{1/9}Fe_{1/9}Mn_{2/3}Ni_{1/9}O_2$ cathode, and its electrochemical performance has been studied in detail. To understand the evolution and impact of this electrolyte on interphases, both anode (SEI) and cathode (cathode electrolyte interphase - CEI) electrodes were thoroughly investigated using Scanning electron microscopy (SEM) and XPS.

2. Experimental

2.1. Electrolyte preparation

To prepare the electrolyte, the received conducting salts NaFSI (Solvionic, 99.9 %, water 20 ppm max) and NaDFOB (Sigma Aldrich, >99 %) were dried at 80 °C in Büchi glass oven under vacuum for 24 h. The PC solvent (Sigma Aldrich, anhydrous,99.7 %) was also dried before electrolyte preparation by using 3 Å molecular sieves for at least 3 days. Inside an argon filled glovebox (MBraun, with H_2O and O_2 contents <1 ppm), electrolyte was prepared by adding the solvent to pre-dried weighted salts in a volumetric flask. A magnetic stirrer was used to facilitate the dissolution of salts in the solvent at ~200 rpm over the entire night.

2.2. Electrodes preparation

2.2.1. Cathode material synthesis & characterization

This work utilizes the same cathode active material (CAM) as our previous publication [41], which features a detailed description of the synthesis and main characterization results of the used P2-AFMNO CAM. In short, the P2-AFMNO CAM was prepared in a three-step synthesis process by (i) precipitation of a double-layer hydroxide precursor with spherical secondary particles followed by a heat-treatment to transform the double-layer hydroxide precursor to an oxide precursor; (ii) dry-mixing of the oxide precursor with Na_2CO_3 (Sigma Aldrich) in a Na: M molar ratio of 2/3 : 1, where M represents the metals of the oxide precursor (Al, Fe, Ni, Mn); (iii) calcination of that mixture for 10 h at 950 °C in synthetic air (20 vol% O_2 in Ar) using a box furnace (Carbolite Gero). After natural cooling to approximately 200 °C, the material was quickly transferred into a Büchi glass oven, where it was kept overnight at 200 °C and dynamic vacuum (approx. 2×10^{-2} Pa), before being transferred into an Argon-filled Glovebox (MBraun, $H_2O < 0.1$ ppm $O_2 < 0.1$ ppm). Subsequent CAM handling, slurry mixing and electrode casting was performed inside the same glovebox to avoid any detrimental effect arising from prolonged contact with ambient air [42–44]. Structural analysis of the CAM was performed using XRD (Bruker D8 Advance equipped with a Cu X-ray tube and a LynxEye XE-T detector). The obtained diffraction pattern closely matches PDF 00-054-0839 and is well indexed with the hexagonal space group $P6_3/mmc$, indicating a phase pure P2-type [45] material. The chemical composition was analyzed with ICP-OES (Spectro Arcos SOP) using a diluted *aqua regia* solution. The obtained result presented in the form of a layered oxide (A_xMO_2, where A is an alkali metal and M is the sum of the transition metals) [45], is $Na_{0.659}Al_{0.115}Fe_{0.113}Mn_{0.660}Ni_{0.113}O_2$, which is in good accordance with the targeted stoichiometry of $Na_{2/3}Al_{1/9}Fe_{1/9}Mn_{2/3}Ni_{1/9}O_2$.

2.2.2. Cathode electrode preparation

By dispersing the CAM powder, a PVDF binder (Solvay Solef 5130) and a conductive agent (SuperP-Li, Imerys Graphite & Carbon) in the weight ratio 93: 4: 3 in an appropriate amount of anhydrous N-methyl-2-pyrrolidone (Sigma Aldrich), a homogenous slurry was obtained. This slurry was cast on an aluminium current collector foil (Korff AG, thickness 15 μm) using the doctor blade technique. The electrode sheet was calendered using a lab-calendar (Sumeet GmbH) at a temperature of 100 °C, a line pressure of 10 N mm^{-1} and a speed of 1 m min^{-1}. Please note that electrode preparation was performed inside an Ar-filled glovebox except for calendaring, where the electrode sheet was briefly in contact with the ambient air.

2.2.3. Anode electrode preparation

HC electrode sheets were prepared by dispersing a commercial HC powder (Kuranode Hard Carbon material Type 2 with an average particle size (D50) of 5 μm, specific surface area of 6 m^2 g^{-1}, and interlayer spacing d_{002} of 0.38 nm), sodium carboxymethylcellulose (Na-CMC, SunroseMAC500 by Nippon Carbon Co., Ltd.) and styrene-butadiene rubber (SBR, BM-451B by Zeon) binders in a weight ratio of 94.6: 1.8: 3.6, respectively, in an appropriate amount of deionized water. The obtained homogenous slurry was cast on aluminium current collector foils (Korff AG, thickness 15 μm) using the doctor blade technique. A wet-film thickness of 100 μm, resulting in an areal active material loading of ~3.85 mg cm^{-2}, was applied for electrodes used for evaluation of electrolytes in half-cells. For the hard carbon electrodes used in full cells, a wet-film thickness of 200 μm, resulting in an areal active material loading of ~7.15 mg cm^{-2} was applied. The dried electrode sheets were calendered using a lab-calendar (Sumeet GmbH) at a temperature of 40 °C, a line pressure of 3 N mm^{-1} and a speed of 1 m min^{-1}.

2.2.4. Electrochemical cells

Electrodes with a diameter of 12 mm were punched from the calendered P2-AFMNO/HC electrode sheets and subsequently dried in a Büchi glass oven at 80 °C and under dynamic vacuum (5.1×10^{-1} mbar).

2.3. Electrochemical characterization

Galvanostatic cycling: For HC half-cell measurements, 3-electrode cell (Swagelok cells) set up was used. A Na metal disc was used as a counter electrode as well as reference electrode. 12 mm diameter HC electrodes were cut and tested in half-cells between 0.02 and 2 V vs Na^+/Na. For the rate-capability test different C-rates of 0.1C,0.5C and 1C (1C = 200 mAh g^{-1}) were applied with 5 cycles at each current density. All electrochemical measurements in half-cells were conducted at room temperature. For lab-scale NIB full cells, similar 3-electrode cell (Swagelok cells) set up was used, with P2-AFMNO cathode as positive electrode and HC as negative electrode each of 12 mm diameters. Metallic Na was used as a reference electrode. Typically, in a rocking-chair type battery, the balancing of the full cells is carried out with an oversized anode to have N/P > 1 to avoid any possible alkali metal deposition on the anode surface. This N/P ratio is calculated based on the reversible areal capacities (mAh cm^{-2}) of the individual electrodes at a similar current density. The following equation is used to calculate the N/P balancing ratio [46].

$$\mathrm{N}\Big/\mathrm{P\ ratio} = \frac{\textit{Anode reversible areal capacity}}{\textit{Cathode reversible areal capacity}}$$

Where areal capacity units are mAh cm^{-2}.

However, in this work, cathode is serving as an over capacity electrode (N/P < 1) to compensate for the loss of Na^+ after the formation cycle. For full cells two capacity balancing ratios (N:P = ~1:1.4) and (N:P = ~1:1.5) were investigated. Thicker electrodes with cathodes having active material mass loadings of 19.47 mg cm^{-2} & 21.36 mg cm^{-2} and HC with constant mass loading of 7.15 mg cm^{-2} were tested. The measurements for full cells were conducted between difference of cathode and anode potentials, 1.5–4.3 V vs Na^+/Na. For all the cells 150 µl of electrolyte (0.5 M NaFSI+0.5 M NaDFOB in PC) was used with one (Whatman GD/F) glass fiber separator.

2.4. Surface characterization

For surface characterization, the P2-AFMNO cathode and HC anode, after cell disassembly, were washed with propylene carbonate (PC) to remove residual soluble salts, followed by overnight drying in a Büchi glass oven at 60 °C under dynamic vacuum (5.1×10^{-1} mbar). The morphologies of both the P2-AFMNO cathode and HC anode electrodes were examined using high-resolution scanning electron microscopy (FE-SEM, ZEISS) with an acceleration voltage of 3 kV. The chemical composition of SEI and CEI was investigated by means of XPS. The high-resolution C 1s, F 1s, B 1s and O 1s spectra were collected in medium area (100 × 100 µm), using a monochromatic Al Kα source ($h\nu = 1487$ eV, 200 W, 12 kV), with an energy pass of 0.1 eV, and using a Phoibos 150 XPS spectrometer (SPECS) and Dealy Line Detector (Surface Concept), in fixed transmission mode. The depth profiling of the SEI and CEI was conducted by a 5 keV Ar ion gun and a sputtering rate of 0.8 nm min^{-1}. The spectra were fixed by CasaXPS software, using Shirley's background and Voigt line shape.

3. Results and discussion

To realize high performance high voltage NIBs, but more in general metal-ion batteries, it is necessary to select electrolytes that display good transport properties, good thermal stability, large electrochemical stability, the ability to form stable passive layers on the electrodes (SEI and CEI) and, the ability to prevent the degradation of Al current collectors. Additionally, they should also ideally have low fluorine content. As shown in Table 1, the low fluorinated electrolyte 0.5 M NaFSI + 0.5 M NaDFOB in PC displays favorable transport and thermal properties and can prevent the corrosion of Al current collectors. Recently, we showed that it can be successfully utilized in combination with P2-layered oxide cathode operating at 4.3 V vs. Na^+/Na [41]. For these reasons, it can certainly be considered as a promising candidate for the realization of high voltage and low fluorinated NIBs.

3.1. Hard carbon in half-cells: electrochemical characterization

HC is the state-of-the art anode material in NIBs, and therefore, we initially investigated the electrochemical performance of this anodic material with the selected electrolyte. The tests were carried out in half cells using metallic sodium as counter electrode. The cell was initially (dis)charged at 0.05C and, afterwards, the rate capability of the electrode was investigated at various C-rates as depicted in Fig. 1a. As shown, during the initial formation cycle at a slow rate (0.05C), a loss of reversible capacity is observed, attributed to a lower initial Coulombic efficiency (CE), i.e., ~77 %. This suggests the consumption of Na^+ in irreversible processes, such as the formation of SEI and the entrapment or irreversible binding of Na^+ ions within the closed pores of HC host structure [47,48]. The reduction of NaDFOB was observed in the initial cycle below ~1.3 V vs Na^+/Na (Fig. S1 in supporting information (SI)). The addition of NaDFOB salt to the electrolyte aided in improving the mechanical stability of SEI and preventing its dissolution in the electrolyte during subsequent cycles [40,41]. The galvanostatic voltage-capacity profiles, shown in Fig. 1b, represent the characteristic profiles for HC, featuring a slopy region (from ~1 V to 0.1 V vs Na^+/Na) and a distinct low voltage plateau region starting below ~0.1 V vs Na^+/Na. When the C-rate increased from 0.1C to 0.5C and 1C, as expected the decrease in electrode capacity was observed. At 0.5C the HC delivered a capacity of almost 100 mAh g^{-1} as compared to ~200 mAh g^{-1} at 0.1C. This capacity drop might arise due to a relatively lower ionic mobility and slightly higher viscosity of the newly developed low-fluorinated electrolyte than the state-of-the-art electrolyte. A comparison of the electrochemical as well as physico-chemical properties of both electrolytes is available in Table S1and Fig. S2 in supplementary information (SI). For slower C-rates the CE values are in the range of 96–98 %, and for higher C-rates the CE is >99 %.

These findings at 0.1C (~200 mAh g^{-1}) were subsequently utilized in the capacity balancing of full cells. It is important to mention that it requires careful consideration while using NaFSI conducting salt, particularly when evaluating hard carbon (HC) in half-cell studies with sodium metal counter electrode. The interaction between this imide-based salt (NaFSI) and Na metal can pose compatibility challenges, potentially leading to less reproducible results among the cells with identical configurations and set ups [49–51]. This is particularly relevant for the cyclability tests, in which results reproducibility was limited. Consequently, only 30 charge/discharge cycles are presented in Fig. S3. Moreover, since the primary objective of this study is the

Table 1
Summary of the physico-chemical and electro-chemical properties of the electrolyte 0.5 M NaFSI +0.5 M NaDFOB in PC [41].

Electrolyte	Ionic conductivity @ 20 °C (mS cm^{-1})	Viscosity @20 °C (mPa s)	Density @ 20 °C (g cm^{-3})	ESW vs (Na^+/Na)	Anodic stability limit for Al current collector vs (Na^+/Na)
0.5 M NaFSI + 0.5 M NaDFOB in PC	4.8	6.6	1.28	up to 5 V	≥ 4.3 V

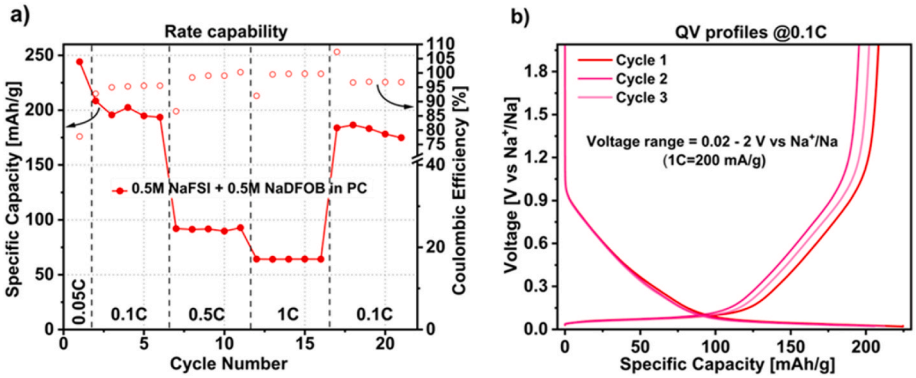

Fig. 1. (a) Hard Carbon rate capability results (5 cycles per C-rate after 1st cycle at 0.05C), and (b) Galvanostatic charge/discharge profiles of HC at 0.1C for the first 3 cycles, using 0.5M NaFSI + 0.5M NaDFOB in PC electrolyte.

development of a functional electrolyte for the lab-scale NIB full cell application, further investigations of the interaction between the NaFSI salt and the Na metal electrode may provide deeper insight into this aspect. Nonetheless, such explorations fall beyond the scope of present work.

3.1.1. *Hard carbon in half-cell: Surface characterization of SEI*

The developed HC in the proposed novel electrolyte (0.5 M NaFSI + 0.5 M NaDFOB in PC) delivers good rate capability and structural reversibility especially at lower C-rates, which are attributed to the presence of NaDFOB and its effect on stabilizing the formed SEI. In this context, XPS analysis was conducted to identify the chemical species formed in the SEI and to understand its stability by measuring after the 1st and 30 cycles, as well as compared with pristine and immersed in the electrolyte HC electrodes. The chemical composition of the formed SEI on cycled HC electrodes was investigated by collecting the C 1s, F 1s, and B 1s photoelectron core-level spectra.

The C 1s spectra (Fig. 2) clearly indicates that the chemical

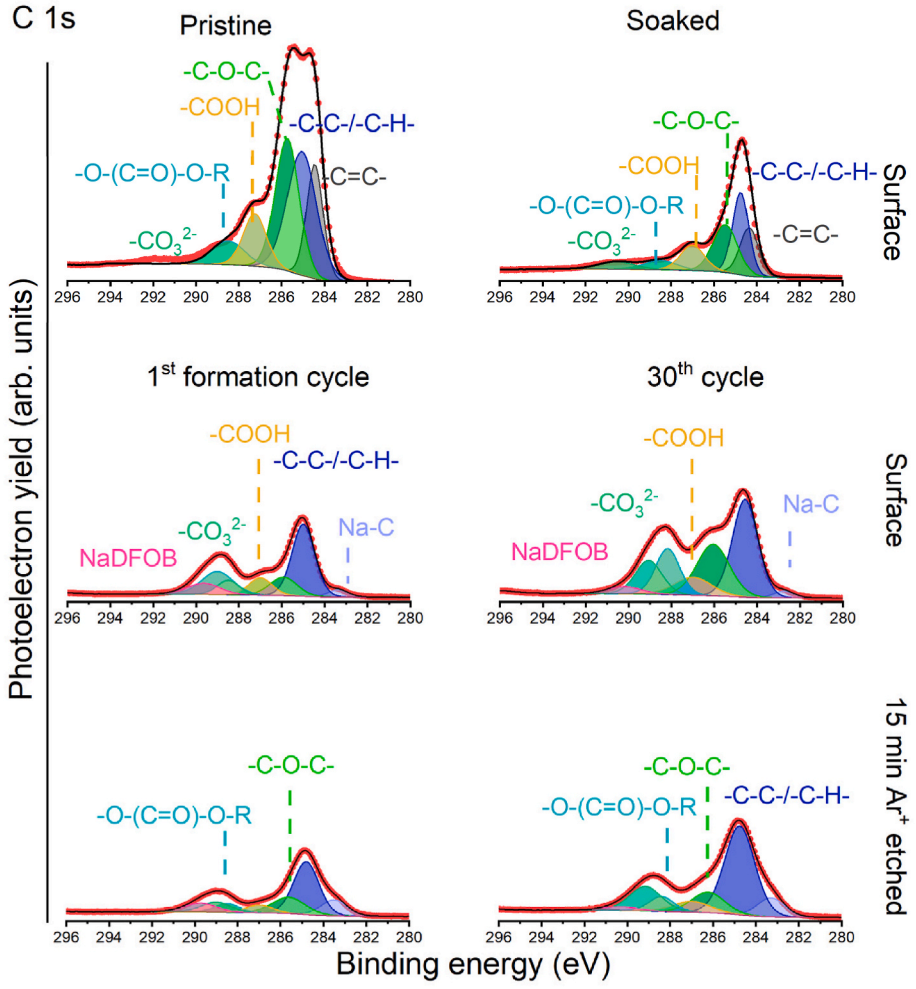

Fig. 2. Chemical composition of the HC anode electrode: C 1s photoelectron core-level of pristine, immersed in the electrolyte, and after 1st and 30th cycle. The cycled HC electrodes were tested at two depths: surface and after etching with Ar^+ for 15 min.

composition of the SEI formed on the cycled HC electrodes is similar in both samples (1st cycle and 30th cycle), showing the presence of Na-C species at low binding energy, corresponding to irreversible Na^+ ions trapped on the HC, as well as hydrocarbons (C-C/C-H at 285.0 eV), ethers (-COC- at 286.0 eV), esters (-COOR at 288.5 eV) and carbonates (CO_3^{2-} at 289.1 eV) most likely arising from the reduction species of PC solvent [52,53]. In addition, decomposition products from the CMC binder (-CH_2-O, at approximately 287.5 eV, as well as certain ethers) and NaDFOB salt (at 289.7 eV) can be found [54]. This is a clear indication that the SEI is formed, in fact, by comparing the C 1s photoelectron region of the pristine electrode and after immersing it in the electrolyte, the -C=C- peak, corresponding to the HC, is reduced, as well as the ethers and -COOH from the binder. In the case of the HC electrode immersed in the electrolyte, lower -C=C- is observed due to salt traces covering the HC electrode surface (see F 1s region in Fig. S4). Meanwhile, the concentration of esters (alkyl carbonates) and carbonates increases upon cycling due to the PC reduction. Indeed, as expected, the concentration of hydrocarbons, alkyl carbonates, and carbonates increases upon cycling, with a higher concentration observed after 30 cycles (16.4 %, 4.7 % and 5.3 % vs. 19.7 %, 6.5 % and 7.5 % of hydrocarbons, alkyl carbonates and carbonates after 1st and 30th cycles, respectively). This is likely due to the continuous reduction of PC, possibly accompanied by the formation and dissolution of the carbonate species in the PC solvent, as previously reported [55]. Nevertheless, the robust inner layer, i.e., close to the electrode, with a lower carbonate concentration, while ethers and NaDFOB are significant (see the SEI after 15 min Ar^+ etching on the 1st formation cycled HC), provides stability to the SEI.

It is interesting to highlight that although the PC in the novel electrolyte (i.e., 0.5 M NaFSI + 0.5 M NaDFOB in PC) is also reduced by forming hydrocarbons, ethers, and (alkyl) carbonates, the concentration of them after the 1st formation cycle is lower than in the HC electrodes tested in conventional electrolyte, i.e., 1 M $NaPF_6$ in EC:PC (tested by our group previously [56]). In addition, the formed SEI after the 1st formation cycle on the surface of the HC electrode tested in a low-fluorinated electrolyte but without NaDFOB (i.e., 1 M NaFSI in EC:PC) is also investigated (see Fig. S6). In this case, the (alkyl) carbonates concentration is not significantly high; however, a higher amount of hydrocarbons is observed. One of the plausible explanation of a carbon-oxygen-richer SEI formed on the HC electrode tested in 1 M $NaPF_6$ in EC:PC and 1 M NaFSI in EC:PC might be due to the fact that in the novel electrolyte (0.5 M NaFSI + 0.5 M NaDFOB in PC) the NaDFOB is also contributing on inner inorganic-rich layer (not only the NaFSI salt), passivating the HC electrode and protecting the surface from further electrolyte decomposition reactions, reducing the decomposition of the solvent. This is in agreement with the higher concentration of -C=C-/Na-C in the conventional and low-fluorinated electrolyte compared with the studied novel electrolyte of this work.

The F 1s region of the cycled HC electrode (1st and 30th cycles) shows the presence of three main components, such as NaFSI and/or its reduction products (F-S bonds at 687.5 eV), NaDFOB and/or its reduced species (B-F at 686.8 eV), and NaF from the reduction of both salts (684.0 eV) [41,57,58]. The absence of NaF on the immersed HC electrodes (Fig. S4) indicates that the reduction of the salts occurs once the current is applied, i.e., upon cycling, and not due to spontaneous chemical reactions between the electrode and electrolyte. Interestingly, after further cycling, the NaF concentration increases, while the peaks corresponding to NaFSI decrease, indicating that NaFSI is more easily reduced to form NaF than NaDFOB, despite its presence remaining significant. More interestingly, and as expected, NaF is mainly located on the surface of the HC electrodes, i.e., in the inner interphase, as confirmed by the F 1s spectrum after etching (15 min Ar^+ etching). This indicated that the NaF in the inner region provides robustness to the SEI.

As shown in Fig. 3, the B 1s region is also analyzed, where the presence of two species is observed after the 1st formation cycle, i.e., F-B at 194.4 eV and B-O at 192.8 eV [59]. The concentration of the latter component, which is formed due to the reduction of NaDFOB (please note that only F-B bond is observed in the HC electrode immersed electrolyte, Fig. S4), is more pronounced at higher SEI depth, or in other words, close to the HC electrode, indicating that NaDFOB also contributes to the SEI formation, mainly forming a non-soluble inner layer. More interestingly, the emergence of new Na-B-O-based species in the SEI layer after the stability test suggests the progressive reduction of NaDFOB during the cycling process. These Na-B-O-based species provide even more inorganic properties to the SEI layer [58]. These results indicate the vital role of the NaDFOB forming inorganic-rich SEI with poor solubility in the carbonate-based electrolyte, similar to those observed for P2-based sodium layered oxide.

Regarding the SEI thickness, the XPS could estimate a rough thickness value considering the photoelectron escape length, inelastic mean free path (IMFP) and the photon energy of specific chemical bonds [60]. In this case, the Na-C peak is observable, which corresponds to the HC electrode; therefore, it could be concluded that the formed SEI is rather thin, thinner than 10 nm, and/or highly inhomogeneous due to the presence of such electrode species. The SEM images (Fig. S5), after the 1st and 30th cycles, display that the HC electrode surface is covered with

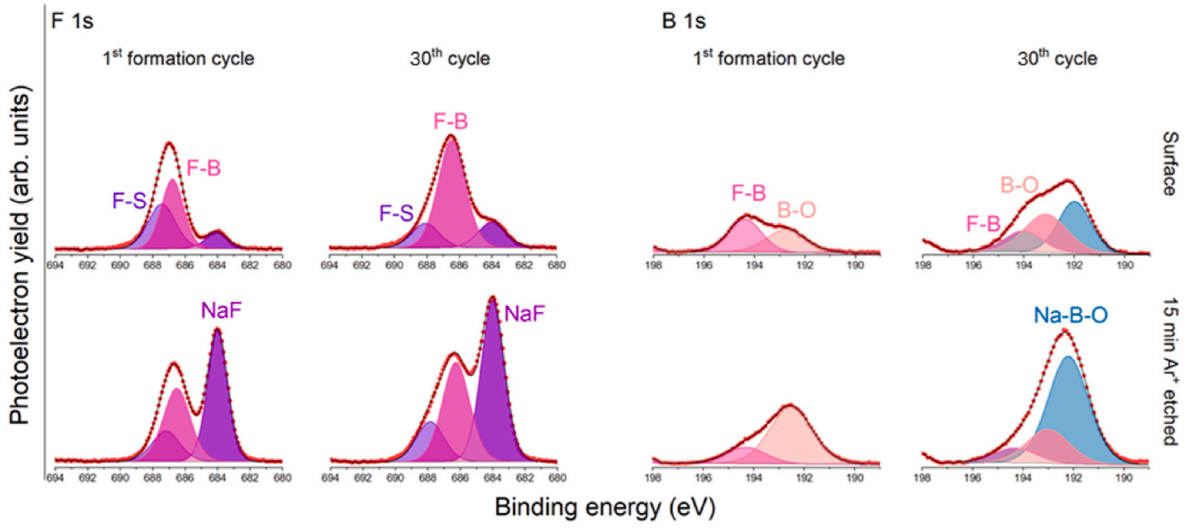

Fig. 3. Chemical composition of the HC anode electrode: F 1s and B 1s photoelectron core-levels after 1st (left) and 30th (right) cycle at two depths: surface (top) and after etching with Ar^+ 15 min (bottom).

deposits. However, due to the resolution of the SEM, it cannot be concluded whether a thin layer covers the particles. Considering the XPS results, it can be hypothesized that a thin inner layer is formed, richer in NaF and NaDFOB-based species, which covers the HC particle. In contrast, more carbonates are formed on the outermost region, which increases upon cycling.

3.2. NIB full cells: Electrochemical characterization

Based on the half-cell results of both HC and high voltage P2-AFMNO cathode (reported in the previous work) [41], a lab-scale NIB full cell containing 0.5 M NaFSI + 0.5 M NaDFOB in PC as the electrolyte was assembled and tested. Table 2 lists the areal capacities of the electrodes and the calculated capacity balancing for full cells. In NIB full cell tests, two different active material mass loadings for layered oxide cathodes (19.47 mg cm^{-2} and 21.36 mg cm^{-2}) corresponding to areal capacities of 1.95 mAh cm^{-2} and 2.14 mAh $cm^{-2,}$ respectively, were investigated. These were paired with constant active material mass loading of HC (7.15 mg cm^{-2}) and an areal capacity of 1.43 mAh cm^{-2}. Two resulting N:P electrodes capacity balancing ratios (~1:1.4 and ~1:1.5) were tested. In the following part, the discussion will exclusively focus on the results obtained for cells with (~1:1.5) ratio, while the information related to (~1:1.4) ratio can be found in Fig. S7 of Supporting Information (SI). In these full cell studies, HC exhibits the limiting capacity, while the cathode is an over-capacity electrode. This over-capacity of the cathode is mainly due to the lower initial CE observed in HC electrodes [61–63]. Consequently, it serves as an effective strategy to compensate for the loss of Na^+ ion inventory during the first few cycles, which is correlated with the irreversible formation of the SEI.

Fig. 4a illustrates the rate capability performance of our laboratory-scale P2-AFMNO-HC full cell. The specific capacity values reported here are based on the HC active material mass. This NIB lab-scale demonstrator cell exhibits a stable rate capability, delivering ca. >255 mAh g^{-1} at 0.1C and >190 mAh g^{-1} at 1C. The initial CE at 0.05C is approximately 109 %. This deviation is attributed to the perturbations in the individual potentials of both electrodes prior to and during the open circuit voltage (OCV) period due to the electrochemical impedance spectroscopy (PEIS) measurement. Further details pertaining to this phenomenon are available in Fig. S8 (left & right) of SI. In subsequent cycles, the CE values range from 98.5 % to 99.6 %, indicating an increase in the reversibility of the cell. C-rate profiles are presented in Fig. 4b. A small discrepancy in the specific capacity values delivered by the cell at 0.1C (in black and red), can be attributed to an increase in cell impedance and thus resulting in overpotential experienced by the cell after the application of higher currents of 1C.

Fig. 4c depicts the cyclability performance of the lab-scaled NIB full cell. This battery demonstrated excellent cycling stability and is able to retain approximately 80 % of its initial capacity after 200 cycles of continuous charge/discharge at 0.5C (1st cycle 223 mAh g^{-1} and 200th cycle 178 mAh g^{-1}). Moreover, the average CE was maintained at >99.5 % during this stability test. The evolution of charge and discharge profiles is displayed in Fig. 4d. These potential curves may provide insights into the possible reasons for the 20 % capacity loss observed over the 200 cycles. During the discharge process, an increment in the cell overpotential due to higher impedance is evident in Fig. 4d (red arrow), which likely contributed to the capacity loss over time. Nevertheless, it is pertinent to note that further optimization of this lab-scale cell, i.e., the thickness of the electrodes and the mass or capacity balancing of the cell, can be beneficial for improving the overall performance. At present, the results obtained encourage the practical feasibility of utilizing these less fluorinated conducting salts electrolytes for NIBs, ensuring efficient performance while maintaining an environmentally benign profile.

Table 2
Overview of areal capacities and capacity balancing (N/P ratios) of full cell electrodes investigated. To calculate the areal capacities and resulting balancing of full cells, 200 mAh g^{-1} and 100 mAh g^{-1} of individual specific capacities were considered for HC and P2-AFMNO layered oxide cathode respectively.

Cathode type	Areal capacity (mAh cm^{-2})	Anode type	Areal capacity (mAh cm^{-2})	Balancing N:P ratio
P2-AFMNO	1.95	HC	1.43	~1:1.4
P2-AFMNO	2.14	HC	1.43	~1:1.5

3.2.1. Surface characterization of SEI & CEI of full cell electrodes

The chemical composition of the formed SEI and CEI onto cycled HC anode and P2-AFMNO cathode electrodes was analyzed by XPS, collecting the C 1s, F 1s, B 1s, and O 1s spectra after the 1st formation and 200th cycles. In addition, as a comparison, the pristine and after-immersion in the electrolyte P2-AFMNO electrodes were also analyzed (for the HC electrode ones, please see the section above).

The C 1s spectrum of the HC electrode after the 1st formation cycle (Fig. 5) shows similar species and composition as observed in the formed SEI on top of the HC when it was tested in half cell configuration (Fig. 2), i.e., Na-C, corresponding to irreversible Na^+ ions trapped on the HC electrode, hydrocarbons (C-C/C-H), ethers (-COC-), esters (-COOR) and carbonates (CO_3^{2-}) from the reduction species of PC solvent, as well as [52,64]-CH_2-O related to the CMC and NaDFOB salts [54]. The main difference is observed after 200 cycles. The C 1s spectrum indicates that the SEI formed in the full cell configuration is thicker or more homogeneously distributed, as the presence of Na-C from the HC electrode is not observable. At the same time, the concentration of hydrocarbons and esters increases due to the further reduction of the PC solvent. The thicker or more homogeneous SEI might be due to the absence of Na metal as a counter electrode, which could influence the stability and species concentration of the SEI by extra side reactions, crosstalk, etc., as indicated by these results [55].

Regarding the C-based species formed in the CEI, in other words the interphase formed on top of P2-AFMNO cathode electrode, the C 1s spectra show similar species as formed on the HC SEI, such as hydrocarbons (C-C/C-H), ethers (-COC-), esters (-COOR) and carbonates (CO_3^{2-}), as well as [52,64] -NaDFOB salts [54]. However, it should be highlighted that the carbon-oxygen species observed in the cycled P2-AFMNO electrodes are already observable in the pristine electrode, indicating the surface reactivity of the P2-AFMNO with the atmosphere. Besides, the P2-AFMNO electrode exhibits a spontaneous chemical reaction with the electrolyte, forming more sodium carbonates on the surface (Fig. S9). Therefore, analyzing the intensity ratio of the peaks, it is suggested that the main species formed after the 1st formation cycle is the alkyl carbonates, mainly on the surface of the PVDF, due to the intensity of -CH_2- and -CF_x-decreases while the intensity of -C=C- (C 1s), corresponding to the conducting carbon remains rather constant, indicating that the CEI is not formed on the surface of the C65.

Additionally, at further electrochemical cycling, the CEI exhibits a similar trend, forming more hydrocarbons and esters upon cycling. However, the C 1s of the P2-AFMNO cathode also display the peaks corresponding to the electrode components, i.e., C=C from the C65 conductive agent, and -CH_2- and -CF_x-from the PVDF binder, after the 1st and 200th cycle. The presence of the species mentioned in the CEI not only after the 1st cycle but also after 200 cycles indicates that the formed CEI is rather thin and/or inhomogeneous, as those species are only observable in the bare P2-AFMNO electrodes (see pristine electrode in Fig. S9). A similar tendency is observed in the O 1s region (Fig. S10), where the peak corresponding to the M − O bonds, i.e., P2-AFMNO, is clearly displayed on the surface region, whose concentration increases at higher depths. Probably, the first hypothesis is more plausible, i.e., CEI is thinner than SEI. Indeed, the SEM images show that the HC is covered by more species upon cycling (Fig. 6), whereas the surface of the P2 electrode remains relatively constant.

Regarding the morphology changes upon cycling, the SEM analysis indicates that the P2-AFMNO cathode remains highly stable after 200

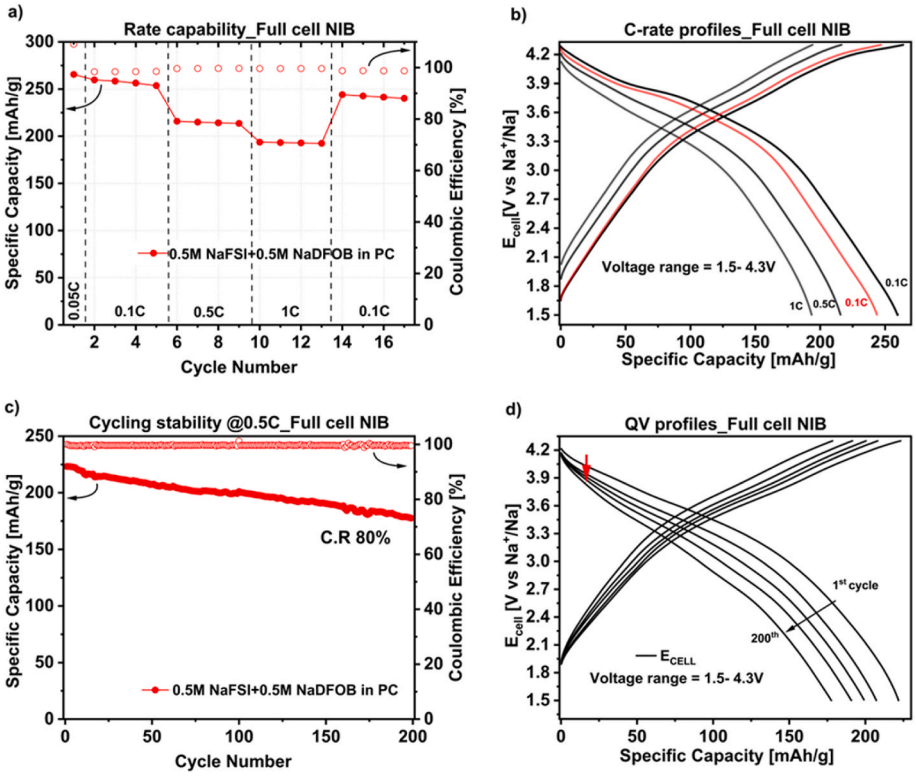

Fig. 4. Electrochemical performance of HC||P2-AFMNO Full cell (N:P = ~1:1.5), at room temperature (a) rate capability results (4 cycles per C-rate after 1st cycle at 0.05C), (b) C-rate profiles of cell voltage at various applied current densities, (c) cyclability test of full cell at 0.5C (after 1st formation cycle at 0.05C and 4 cycles at 0.1C), (d) Capacity voltage profiles evolution of cell voltage during stability test at 0.5C over 200 cycles (1st, 50th,100th, 150th, 200th), using 0.5M NaFSI + 0.5M NaDFOB in PC electrolyte.; C.R= Capacity retention (measured for 1st cycle vs 200th cycle at 0.5C).

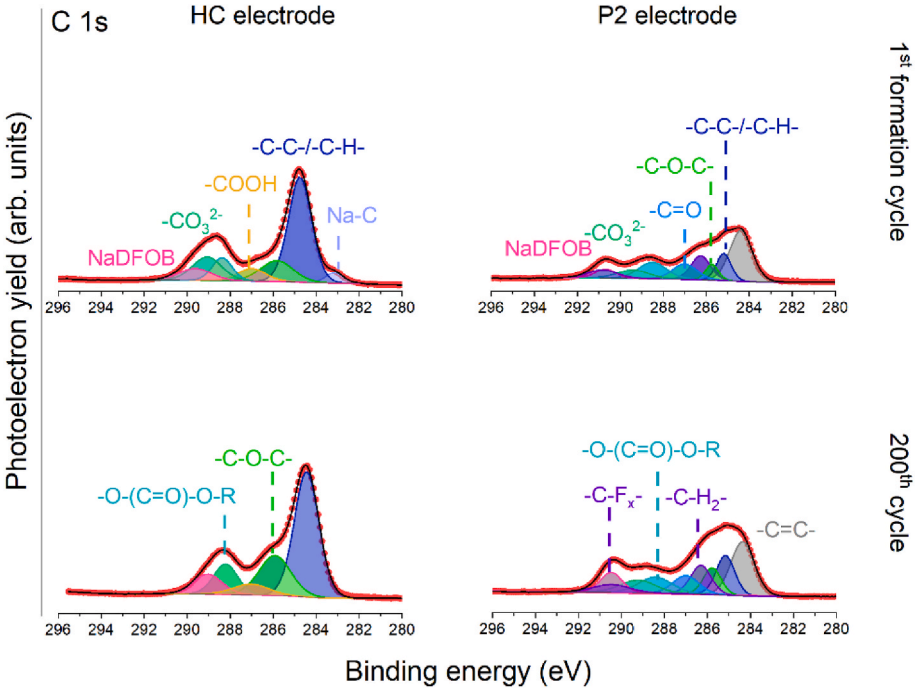

Fig. 5. Chemical composition of the HC anode (left) and P2-AFMNO (right) electrodes: C 1s photoelectron core-level after 1st (top) and 200th (bottom) cycles.

cycles, with no significant morphological changes. The surfaces appear clean and intact, suggesting that the formed CEI is thin and stable. In contrast, in the 1st cycle, the surface of the HC anode electrode exhibits a smooth and uniform morphology. However, the irreversible capacity after long-term cycling may be linked to the presence of an irreversible component on the surface of the HC, as evidenced by white deposits observed after the 200th cycle and the presence of additional esters and hydrocarbons in the C 1s region. Please note that the newly formed

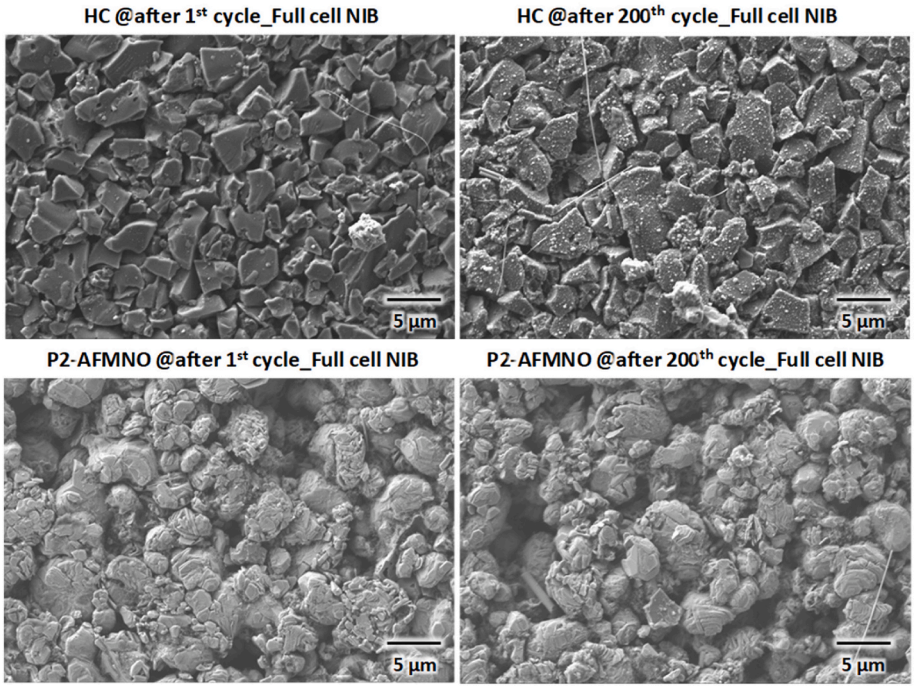

Fig. 6. SEM images of full cell electrodes.

species on the surface of the HC electrodes are not related to Na metal deposits, as indicated by the absence of Na metal surface and bulk plasmon on the Na 1s photoelectron region (Fig. S11). The fibers present on the HC surface, shown in the SEM images, are the separator fibers de-attached from the separator during the disassembly process of the cell for the post-mortem analysis.

The F 1s and B 1s regions (Fig. 7) illustrate the decomposition reactions of both salts, i.e., NaFSI and NaDFOB. Indeed, the SEI and CEI display the presence of NaFSI and its reduction species, NaDFOB, as well as its decomposition products, and NaF. In the 1st formation cycles, more interestingly, the SEI is richer in B-based decomposition products from the NaDFOB, while the CEI is mainly composed of NaFSI and NaF, which are also already formed during the electrode preparation (pristine electrode) and in contact with the electrolyte (immersed electrode – see Fig. S9). Hence, these results clearly demonstrate that the NaDFOB is more easily reduced on the surface of the HC anode electrode, while NaFSI reacts on the cathode interface. Additionally, the presence of higher concentrations of NaF in the CEI may be related to the fact that the P2-AFMNO electrode is based on a PVDF binder, and it is known that PVDF suffers from dehydrofluorination in the presence of small traces of water or basic media, as indicated by the pristine and immersed electrodes. Therefore, the formation of NaF could be due to the reduction of NaFSI, as well as the dehydrofluorination of PVDF [55,65].

After the 200th cycle, the SEI is rather similar, showing NaFSI and NaDFOB species, as well as their decomposition products in both F 1s and B 1s regions. However, in the case of the CEI of the P2-AFNMO electrode, the CEI slightly evolved upon cycling, exhibiting more B-based species, likely due to the further decomposition of NaDFOB upon

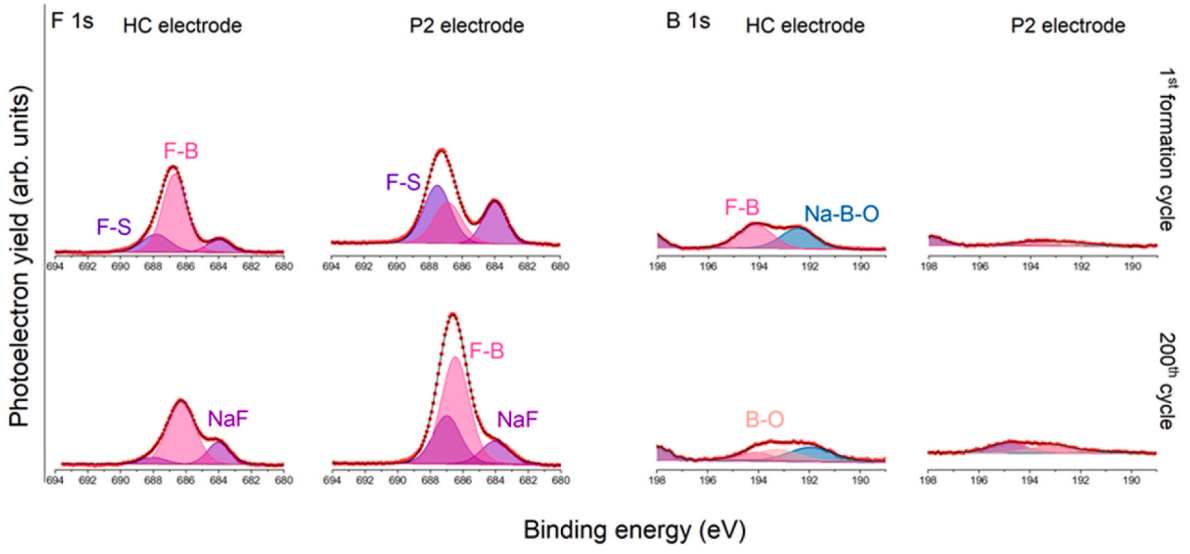

Fig. 7. Chemical composition of the HC anode (left) and P2-AFMNO (right) electrodes: F 1s (right) and B 1s (left) photoelectron core-levels after 1st (top) and 200th (bottom) cycle.

cycling, which also contributes to the formation of an inorganic-richer CEI.

4. Conclusion

This research work focuses on the development of low-fluorinated electrolyte, formulated with NaFSI and NaDFOB salts in carbonated PC solvent (0.5 M NaFSI + 0.5 M NaDFOB in PC), and its subsequent electrochemical characterization in HC based half-cells and later in full cells (employing HC anode vs P2-$Na_{2/3}Al_{1/9}Fe_{1/9}Mn_{2/3}Ni_{1/9}O_2$ cathode). Lab-scale NIB demonstrator cell incorporating this high voltage layered oxide cathode and cycled at 4.3 V, demonstrated robust cycling performance achieving ~80 % retention in capacity over 200 cycles. These findings not only underscore the encouraging electrochemical performance of the battery but also highlight the environmental benefits of the electrolyte, attributed to its reduced fluorine content compared to the state-of-the-art $NaPF_6$ -based electrolytes. Comprehensive post-mortem analysis of the full cell, based on spectroscopy (XPS) and microscopy (SEM) was carried out to assess the composition of interphases as well as morphological changes of particles, before and after 200 cycles. These investigations revealed the formation of stable, inorganic-rich interphases on both electrodes and minimal changes in particles morphology, particularly evident on P2-AFMNO cathode. Consequently, the promising performance in NIB demonstrator cell strongly supports the rational design of such low-fluorinated electrolytes for energy storage applications especially for NIBs.

CRediT authorship contribution statement

Muhammad Nouman Aslam: Writing – original draft, Investigation. **Yiyue Lu:** Investigation. **Shuting Zhang:** Investigation. **Mariana Gaško:** Investigation. **Maider Zarrabeitia:** Writing – review & editing, Investigation, Funding acquisition. **Lukas Fridolin Pfeiffer:** Investigation. **Timo Werner:** Investigation. **Peter Axmann:** Writing – review & editing, Funding acquisition. **Christian Leibing:** Investigation. **Andrea Balducci:** Writing – review & editing, Supervision, Funding acquisition.

Declaration of competing interest

The authors declare that they have no known competing financial interests or personal relationships that could have appeared to influence the work reported in this paper.

Acknowledgements

The authors wish to thank the Bundesministerium für Bildung und Forschung for the financial support with the project „TransitionTransfer - Natrium-lonen Batterie Demonstratoren fur mobile und stationare Energiespeicher" (03XP0533A, 03XP0533B, 03XP0533C and 03XP0533D).

Appendix A. Supplementary data

Supplementary data to this article can be found online at https://doi.org/10.1016/j.jpowsour.2025.238548.

Data availability

Data will be made available on request.

References

[1] P. Phogat, S. Dey, M. Wan, Mater. Sci. Eng., B 312 (2025) 117870.
[2] Z. Xu, J. Wang, Adv. Energy Mater. 12 (2022) 2201692.
[3] T. Liu, Y. Zhang, Z. Jiang, X. Zeng, J. Ji, Z. Li, X. Gao, M. Sun, Z. Lin, M. Ling, Energy Environ. Sci. 12 (2019) 1512–1533.
[4] A.N. Singh, M. Islam, A. Meena, M. Faizan, D. Han, C. Bathula, A. Hajibabaei, R. Anand, K.W. Nam, Adv. Funct. Mater. 33 (2023) 2304617.
[5] K. Abraham, ACS Energy Lett. 5 (2020) 3544–3547.
[6] C. Vaalma, D. Buchholz, M. Weil, S. Passerini, Nat. Rev. Mater. 3 (2018) 1–11.
[7] S. Lilley, Faraday Insights, 2021, p. 11.
[8] A. Rudola, R. Sayers, C.J. Wright, J. Barker, Nat. Energy 8 (2023) 215–218.
[9] H. Pan, Y.-S. Hu, L. Chen, Energy Environ. Sci. 6 (2013) 2338–2360.
[10] H.S. Hirsh, Y. Li, D.H. Tan, M. Zhang, E. Zhao, Y.S. Meng, Adv. Energy Mater. 10 (2020) 2001274.
[11] N. Yabuuchi, K. Kubota, M. Dahbi, S. Komaba, Chem. Rev. 114 (2014) 11636–11682.
[12] C. Fang, Y. Huang, W. Zhang, J. Han, Z. Deng, Y. Cao, H. Yang, Adv. Energy Mater. 6 (2016) 1501727.
[13] S.W. Kim, D.H. Seo, X. Ma, G. Ceder, K. Kang, Adv. Energy Mater. 2 (2012) 710–721.
[14] X. Xiang, K. Zhang, J. Chen, Adv. Mater. 27 (2015) 5343–5364.
[15] T. Chen, B. Ouyang, X. Fan, W. Zhou, W. Liu, K. Liu, Carbon Energy 4 (2022) 170–199.
[16] Y.B. Niu, Y.J. Guo, Y.X. Yin, S.Y. Zhang, T. Wang, P. Wang, S. Xin, Y.G. Guo, Adv. Mater. 32 (2020) 2001419.
[17] Y.-U. Park, D.-H. Seo, H.-S. Kwon, B. Kim, J. Kim, H. Kim, I. Kim, H.-I. Yoo, K. Kang, J. Am. Chem. Soc. 135 (2013) 13870–13878.
[18] H. Li, M. Xu, Z. Zhang, Y. Lai, J. Ma, Adv. Funct. Mater. 30 (2020) 2000473.
[19] Y. You, A. Manthiram, Adv. Energy Mater. 8 (2018) 1701785.
[20] Q. Liu, Z. Hu, M. Chen, C. Zou, H. Jin, S. Wang, S.L. Chou, S.X. Dou, Small 15 (2019) 1805381.
[21] Q. Liu, Z. Hu, W. Li, C. Zou, H. Jin, S. Wang, S. Chou, S.-X. Dou, Energy Environ. Sci. 14 (2021) 158–179.
[22] A. Ponrouch, D. Monti, A. Boschin, B. Steen, P. Johansson, M.R. Palacín, J. Mater. Chem. A 3 (2015) 22–42.
[23] Y. Huang, L. Zhao, L. Li, M. Xie, F. Wu, R. Chen, Adv. Mater. 31 (2019) 1808393.
[24] K. Vignarooban, R. Kushagra, A. Elango, P. Badami, B.-E. Mellander, X. Xu, T. Tucker, C. Nam, A.M. Kannan, Int. J. Hydrogen Energy 41 (2016) 2829–2846.
[25] J. Zhang, J. Li, H. Wang, M. Wang, Front. Chem. 11 (2023) 1253959.
[26] M. He, A.E. Mejdoubi, D. Chartouni, M. Morcrette, P. Troendle, R. Castiglioni, J. Power Sources 588 (2023) 233741.
[27] P. Desai, J. Forero-Saboya, V. Meunier, G. Rousse, M. Deschamps, A.M. Abakumov, J.-M. Tarascon, S. Mariyappan, Energy Storage Mater. 57 (2023) 102–117.
[28] A. Rudola, A.J. Rennie, R. Heap, S.S. Meysami, A. Lowbridge, F. Mazzali, R. Sayers, C.J. Wright, J. Barker, J. Mater. Chem. A 9 (2021) 8279–8302.
[29] K. Tang, Y. Ren, Sodium-ion batteries: materials, Character. Technol. 2 (2022) 531–549.
[30] Y. Jin, P.M. Le, P. Gao, Y. Xu, B. Xiao, M.H. Engelhard, X. Cao, T.D. Vo, J. Hu, L. Zhong, Nat. Energy 7 (2022) 718–725.
[31] C.L. Campion, W. Li, B.L. Lucht, J. Electrochem. Soc. 152 (2005) A2327.
[32] N.P. Lebedeva, L. Boon-Brett, J. Electrochem. Soc. 163 (2016) A821.
[33] F. Larsson, P. Andersson, P. Blomqvist, B.-E. Mellander, Sci. Rep. 7 (2017) 10018.
[34] R. Fuge, Appl. Geochem. 100 (2019) 393–406.
[35] L.O.S. Colbin, C.A. Hall, A.S. Etman, A. Buckel, L. Nyholm, R. Younesi, in: Electrochemical Society Meeting Abstracts 244, the Electrochemical Society, Inc., 2023, 3054-3054.
[36] L. Otaegui, E. Goikolea, F. Aguesse, M. Armand, T. Rojo, G. Singh, J. Power Sources 297 (2015) 168–173.
[37] J. Chen, Z. Huang, C. Wang, S. Porter, B. Wang, W. Lie, H.K. Liu, Chem. Commun. 51 (2015) 9809–9812.
[38] X. Liu, J. Zhao, H. Dong, L. Zhang, H. Zhang, Y. Gao, X. Zhou, L. Zhang, L. Li, Y. Liu, Adv. Funct. Mater. 34 (2024) 2402310.
[39] M. Xia, H. Chen, Z. Zheng, Q. Meng, A. Zhao, X. Chen, X. Ai, Y. Fang, Y. Cao, Adv. Energy Mater. (2024) 2403306.
[40] L. Huang, Q. Qiu, M. Yang, H. Li, J. Zhu, W. Zhang, S. Wang, L. Xia, P. Müller-Buschbaum, ACS Appl. Mater. Interfaces 16 (2024) 46392–46400.
[41] Y. Lu, M.N. Aslam, C. Leibing, M. Zarrabeitia, L. Roselli, L.F. Pfeiffer, P. Axmann, J. Geisler, P. Adelhelm, A. Balducci, Small (2025) 2410704.
[42] W. Zuo, A. Innocenti, M. Zarrabeitia, D. Bresser, Y. Yang, S. Passerini, Acc. Chem. Res. 56 (2023) 284–296.
[43] W. Zuo, J. Qiu, X. Liu, F. Ren, H. Liu, H. He, C. Luo, J. Li, G.F. Ortiz, H. Duan, Nat. Commun. 11 (2020) 3544.
[44] W. Zuo, Z. Xiao, M. Zarrabeitia, X. Xue, Y. Yang, S. Passerini, ACS Mater. Lett. 4 (2022) 1074–1086.
[45] C. Delmas, C. Fouassier, P. Hagenmuller, Physica B+C 99 (1980) 81–85.
[46] Y. Son, H. Cha, C. Jo, A.S. Groombridge, T. Lee, A. Boies, J. Cho, M. De Volder, Mater. Today Energy 21 (2021) 100838.
[47] C. Leibing, D. Leistenschneider, C. Neumann, M. Oschatz, A. Turchanin, A. Balducci, ChemSusChem 16 (2023) e202300161.
[48] C. Ren, J. He, H. Xu, J. Wang, K. Li, K. Hu, L. Zhao, H. Wang, R. Yang, Electrochim. Acta (2025) 145968.
[49] K. Pfeifer, S. Arnold, J. Becherer, C. Das, J. Maibach, H. Ehrenberg, S. Dsoke, ChemSusChem 12 (2019) 3312–3319.
[50] J. Conder, C. Villevieille, Chem. Commun. 55 (2019) 1275–1278.
[51] R. Dugas, A. Ponrouch, G. Gachot, R. David, M.R. Palacín, J.-M. Tarascon, J. Electrochem. Soc. 163 (2016) A2333.
[52] H. Moon, M. Zarrabeitia, E. Frank, O. Böse, M. Enterría, D. Saurel, I. Hasa, S. Passerini, Batteries Supercaps 4 (2021) 960–977.
[53] M.C. Biesinger, in, Oxford University Press US, 2024..
[54] M. Dahbi, T. Nakano, N. Yabuuchi, T. Ishikawa, K. Kubota, M. Fukunishi, S. Shibahara, J.-Y. Son, Y.-T. Cui, H. Oji, Electrochem. Commun. 44 (2014) 66–69.

[55] M.A. Muñoz-Márquez, M. Zarrabeitia, E. Castillo-Martínez, A. Eguía-Barrio, T. Rojo, M. Casas-Cabanas, ACS Appl. Mater. Interfaces 7 (2015) 7801–7808.
[56] M. Gaško, C. Leibing, L. Fridolin Pfeiffer, P. Axmann, A. Balducci, M. Zarrabeitia, Chemelectrochem (2025) 2500162.
[57] M. Zarrabeitia, L. Gomes Chagas, M. Kuenzel, E. Gonzalo, T.f. Rojo, S. Passerini, M. A.n. Muñoz-Márquez, ACS Appl. Mater. Interfaces 11 (2019) 28885–28893.
[58] A. Selka, A. Abidli, L. Schiavo, L. Jeanmart, G. Hanquet, W.D. Lubell, Eur. J. Org Chem. 28 (2025) e202400983.
[59] Q. Zhang, Z. Wang, X. Li, H. Guo, J. Wang, G. Yan, Ionics 27 (2021) 683–691.
[60] S. Tanuma, C. Powell, D. Penn, Relat. Phenom. 40 125 (1 986) (1991) 17.
[61] B. Yang, J. Wang, Y. Zhu, K. Ji, C. Wang, D. Ruan, Y. Xia, J. Power Sources 492 (2021) 229656.
[62] Y. Yang, C. Wu, X.X. He, J. Zhao, Z. Yang, L. Li, X. Wu, L. Li, S.L. Chou, Adv. Funct. Mater. 34 (2024) 2302277.
[63] M.K. Rybarczyk, Y. Li, M. Qiao, Y.-S. Hu, M.-M. Titirici, M. Lieder, J. Energy Chem. 29 (2019) 17–22.
[64] M.C. Biesinger, Appl. Surf. Sci. 597 (2022) 153681.
[65] G.G. Eshetu, T. Diemant, M. Hekmatfar, S. Grugeon, R.J. Behm, S. Laruelle, M. Armand, S. Passerini, Nano Energy 55 (2019) 327–340.